JOURNAL OF THERMOPHYSICS AND HEAT TRANSFER
Vol. 11, No. 4, October–December 1997

Bounded, High-Resolution Differencing Schemes Applied to the Discrete Ordinates Method

J. Patrick Jessee* and Woodrow A. Fiveland†
Babcock and Wilcox, Alliance, Ohio 44601

This paper presents an improved spatial differencing practice for the discrete ordinates form of the radiative transport equation (RTE). Several bounded, high-resolution (HR) schemes are applied to the primitive variable form of the RTE in a finite volume context. These schemes provide high accuracy while removing nonphysical oscillations that are characteristic of the diamond difference scheme. A defect correction technique is applied to solve the equations that result from the high-order operators. Predictions from the HR schemes are compared to those of the conventional step and diamond difference schemes for a number of two-dimensional enclosures with gray walls, and either absorbing or isotropically scattering media. Accuracy, stability, and effects on convergence are addressed for the different schemes. The HR schemes were found to provide both accuracy and boundedness at modest computational costs.

Nomenclature

A = area, m^2
C = constant
E = error, %
e = error
$\boldsymbol{F}$ = right-hand-side vector of discrete transport equation
f = general interpolation function
G = incident energy, $\int_{4\pi} I(\boldsymbol{r}, \Omega)\, d\Omega$, W/m^2
I = intensity, $W/m^2 \cdot sr$
K = discrete transport operator
L = continuous transport operator
M = total number of ordinate directions
N = number of control volumes in computation mesh
$\boldsymbol{n}$ = surface normal
p = predicted spatial approximation order
R = residual
$\boldsymbol{r}$ = position vector, m
S = source term, W/m^3-sr
S_n = order of discrete ordinates approximation
V = volume, m^3
w_k = direction weights
x, y = coordinate directions, m
$\boldsymbol{\beta}$ = extinction coefficient, $\kappa + \sigma$, m^{-1}
Γ = domain boundary
Δx = uniform control volume size, m
ε = emissivity
κ = absorption coefficient, m^{-1}
μ, ξ, η = direction cosines
ρ = reflectivity, $1 - \varepsilon$
σ = scattering coefficient, m^{-1}
$\boldsymbol{\Omega}$ = direction with direction cosines, μ, ξ, η

Subscripts
b = blackbody
C, D, U = local indices in nodal stencil
f, uf = local face indices
i, j = nodal indices
k = generic index
m = direction
n = nth S_n approximation
∞ = infinity norm

Superscripts
HR = high-resolution scheme
n = iteration
1 = first-order scheme

Special Symbols
$-$ = exact value
$'$ = dummy variable of integration
$\sim$ = normalized quantity
$\|\cdot\|$ = norm

Received Sept. 3, 1996; revision received Feb. 19, 1997; accepted for publication April 7, 1997.

*Research Engineer, Numerical Modeling Section, Research and Development Division, 1562 Beeson Street. E-mail: patrick.jessee@mcdermott.com. Member AIAA.

†Manager, Numerical Modeling Section, Research and Development Division, 1562 Beeson Street. Senior Member AIAA.

I. Introduction

METHODS for the numerical solution of the radiative transport equation (RTE) in multidimensional geometries have greatly expanded over the past two decades. Of the various methods, fixed angle methods (FAMs), including the discrete ordinates[1,2] and finite element angular[3] approximations, have gained wide acceptance because of several desirable characteristics: they are deterministic, conservation of radiant energy can be obtained to machine round-off, and they can easily be extended to higher-order approximations.

The solution of the RTE by FAMs requires discretization of both spatial and angular domains. Generally, the name of the FAM denotes the angular approximation technique. For instance, the discrete ordinates (DO) method generally denotes the use of an S_n angular approximation. Spatial discretization may be accomplished with a variety of techniques including finite volume, finite element, and nodal[4] methods. For most FAMs, the angular and spatial discretization methods may be independent. Both mixed and homogeneous discretization techniques have been employed for the angular and spatial domains. Examples of mixed approximations include discrete ordinate/finite volume formulations[2,5,6] and discrete ordinate/finite element formulations.[3,7] Conversely, examples of homogeneous approximations include: finite element/finite element formulations[3] and finite angle (piecewise constant)/finite volume formulations.[8–10] (The finite angle and piecewise

constant angular approximations are conceptually the same, and both satisfy the half-range first moment exactly. Fiveland and Jessee[10] reported that the piecewise constant method does not satisfy this moment. This statement was based on an implementation that did not integrate the direction cosines over the discrete solid angles exactly; if an analytic angular integration method is used, the moment is satisfied.)

The accuracy of the resulting RTE approximation obviously depends on the accuracy of both the angular and spatial approximations. Angular discretization error often takes the form of ray effects,[11] which are more prevalent at low optical thicknesses and low levels of scattering. These errors may be mitigated with higher-order angular approximations. For the case of the DO method, this is accomplished with a higher-order S_n set, whereas for the finite element method, this is achieved with a higher degree of angular discretization and/or a higher-order polynomial basis.

Spatial discretization (SD) error, the topic of this paper, takes the form of numerical smearing and dispersion. Numerical smearing results from local truncation error that is associated with 1) low-order methods such as the first-order step scheme and/or 2) schemes with interpolation stencils that are not aligned with ordinate directions. (Numerical smearing has been referred to as numerical scattering.[12] Although low-order spatial operators appear to be mimicking the physical process of scattering, it is fundamentally a different phenomenon for which there is no physical analog. The low-order spatial operators do not cause scattering of rays into other directions; they redistribute the energy within a given ordinate direction. For this reason the authors have adopted the term numerical smearing.) Numerical dispersion, on the other hand, takes the form of nonphysical over- and undershoots, and results from unbounded discretization schemes. The elimination of both the numerical smearing and dispersion is usually difficult. Smearing may be reduced by resorting to a higher-order spatial approximation or to a finer grid. Unfortunately, the higher-order scheme commonly introduces dispersion, and the finer grid increases computational and memory requirements. Conversely, dispersion of higher-order methods may be eliminated by using a lower-order method, but at the price of smearing.

The optimum SD scheme provides high-order accuracy and prevents nonphysical over- and undershoots. Both the computational fluid dynamics (CFD) and neutron transport communities have worked toward developing such discretization schemes for first-order transport operators. One of the most promising approaches in the CFD community has been the class of bounded, high-resolution (HR) schemes.[13,14] These schemes are generally composed of a high-order interpolation scheme and a flux limiter that enforces boundedness. An initial investigation of bounded HR schemes for the RTE has been performed by Fiveland and Jessee.[10] Schemes similar in spirit have recently been developed in the neutron transport community by Alcouffe[15] and Germogenova et al.[16]

The objectives of this paper are the following:

1) To formally extend bounded HR schemes to the discretization of the RTE.

2) To investigate the behavior of these schemes for several problems.

3) To propose future directions for development of differencing operators for the RTE.

A number of bounded HR schemes are applied in a DO context. Although presented from a DO vantage point, these schemes may be generally applied to other angular approximations. The remainder of the paper is broken into four sections: Section II presents the governing equations (the radiative transport equation and DO approximation); Sec. III details spatial discretization schemes; Sec. IV presents results from the schemes; and lastly, Sec. V summarizes the work and states conclusions based on the considered cases.

II. Governing Equations

A. Radiative Transport Equation

This paper considers an emitting–absorbing and isotopically scattering gray medium. For this medium, the RTE is

$$(\boldsymbol{\Omega}\cdot\nabla)I(\boldsymbol{r},\boldsymbol{\Omega}) = -(\kappa+\sigma)I(\boldsymbol{r},\boldsymbol{\Omega}) + \frac{\sigma}{4\pi}\int_{4\pi} I(\boldsymbol{r},\boldsymbol{\Omega}')\,\mathrm{d}\boldsymbol{\Omega}' + \kappa I_b(\boldsymbol{r}) \tag{1}$$

where $I(\boldsymbol{r},\boldsymbol{\Omega})$ is the radiation intensity at position $\boldsymbol{r}$, and traveling in direction $\boldsymbol{\Omega}$; $I_b(\boldsymbol{r})$ is the intensity of blackbody radiation at the temperature of the medium; κ and σ are the gray absorption and scattering coefficients of the medium, respectively; and the integration is performed over the incident directions $\boldsymbol{\Omega}'$.

For gray surfaces that reflect diffusely, the radiative boundary condition for Eq. (1) is given by

$$I(\boldsymbol{r},\boldsymbol{\Omega}) = \varepsilon I_b(\boldsymbol{r}) + \frac{\rho}{\pi}\int_{\boldsymbol{n}\cdot\boldsymbol{\Omega}'<0} |\boldsymbol{n}\cdot\boldsymbol{\Omega}'|\,I(\boldsymbol{r},\boldsymbol{\Omega}')\,\mathrm{d}\boldsymbol{\Omega}' \tag{2}$$

where $\boldsymbol{r}$ belongs to Γ, and Eq. (2) applies for $\boldsymbol{n}\cdot\boldsymbol{\Omega} > 0$. $I(\boldsymbol{r},\boldsymbol{\Omega})$ is the intensity leaving a surface at a boundary condition location, ε is the surface emissivity, ρ is the surface reflectivity, and $\boldsymbol{n}$ is the unit normal vector at the boundary location.

B. DO Method

In the DO method, the governing RTE is replaced by a discrete set of M equations for a finite number of directions, $\boldsymbol{\Omega}_m$, and each integral is replaced by a quadrature:

$$(\boldsymbol{\Omega}_m\cdot\nabla)I(\boldsymbol{r},\boldsymbol{\Omega}_m) = -\beta I(\boldsymbol{r},\boldsymbol{\Omega}_m) + \frac{\sigma}{4\pi}\sum_{k=1}^{M} w_k I(\boldsymbol{r},\boldsymbol{\Omega}_k) + \kappa I_b \tag{3}$$

where w_k are the ordinate weights.[5,17] This angular approximation transforms the original integro-differential equation into a set of coupled differential equations.

The notation in Eq. (3) may be simplified as follows:

$$L_m(I_m) = \kappa I_b + S_m \tag{4}$$

where S_m denotes the in-scattering source term, and the linear operator L_m is defined as

$$L_m = (\boldsymbol{\Omega}_m\cdot\nabla) + \beta \tag{5}$$

After angular discretization has been performed, the DO equations may be discretized spatially. Spatial approximation is detailed in the following section.

III. Numerical Methods

A. Finite Volume Discretization

The DO equations are spatially discretized using standard cell-centered, finite volume techniques. All formulations in this paper are based on structured, uniform grids and Cartesian coordinates. An unstructured grid formulation is outlined in a previous work.[10] The spatially discrete ordinate equation is obtained by integrating Eq. (3) over a typical control volume (Fig. 1):

$$\mu_m A_x(I_{m,i+1/2,j} - I_{m,i-1/2,j}) + \xi_m A_y(I_{m,i,j+1/2} - I_{m,i,j-1/2}) = V_{i,j}(\kappa I_b - \beta I_m + S_m)_{i,j} \tag{6}$$

As shown in Fig. 1a, half indices denote face values, whereas integral indices denote nodal or in-cell values. Similar equations may be written for all control volumes within the grid.

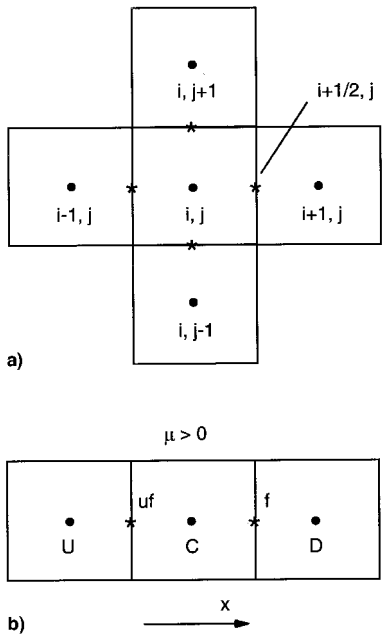

Fig. 1 Stencils for finite volume discretization: a) two-dimensional stencil with global indices and b) unidirectional stencil for face interpolation.

Assuming that boundary conditions are given, the system of equations is closed by defining an interpolation scheme that relates the face intensities to the nodal values.

B. General Face Interpolation Scheme

This paper considers a number of unidirectional interpolation schemes that range from first to third order. For these schemes, the interpolation at a given face involves no more than three nodal values, and can be generalized by a three-point stencil. Graphically, the stencil is shown in Fig. 1b for face f (global face $i + 1/2, j$). The corresponding face intensity may be expressed as

$$I_f = f(I_U, I_C, I_D) \tag{7}$$

where the ordinate direction subscript m has been omitted from Eq. (7) for clarity. The orientation of the nodal stencil relative to the face is determined by the sign of the dot product of ordinate direction and the face normal vector. For orthogonal grids, this is equivalent to inspecting the sign of the corresponding direction cosine. Orders higher than third may be applied, but such schemes have larger stencils, and comparisons have shown diminishing returns with respect to the solution accuracy/CPU time ratio.

For purposes of applying the bounded HR schemes, the general interpolation expression is rewritten using the normalized variable formulation (NVF) of Leonard[18]:

$$\tilde{I}_f = f(\tilde{I}_C) \tag{8}$$

The normalized variables, denoted with tildes, are defined as

$$\tilde{I} = (I - I_U)/(I_D - I_U) \tag{9}$$

The NVF has been extended to nonuniform discretizations by Darwish and Moukalled,[19] but because only uniform discretizations are employed in this paper, this extension is not required here. The unnormalized face intensity may be recovered by rearrangement of Eq. (9).

C. Monotonicity-Maintenance Criteria

The conditions for ensuring boundedness from the discretization of first-order operators are detailed by Leonard[13] and Gaskell and Lau.[20] These conditions are briefly reviewed here in the context of the DO equation.

First, monotonic behavior requires that the intensity at a face be bounded by intensities at adjacent nodes. This is referred to as interpolative boundedness, and in normalized variables, translates into the following condition:

$$\tilde{I}_C \le \tilde{I}_f \le 1 \quad \text{for} \quad 0 \le \tilde{I}_C \le 1 \tag{10}$$

The second condition states that if a nodal value is not in the monotonic range, then the face value is restricted to the upstream nodal value:

$$\tilde{I}_f = \tilde{I}_C \quad \text{for} \quad \tilde{I}_C \notin [0,1] \tag{11}$$

This condition is needed to provide computed boundedness in the presence of emission and in-scattering sources that may cause valid local extrema. The second condition is equivalent to first-order upwinding or the step approximation; however, the overall accuracy of the method is generally not corrupted because this limiting, if required, is usually restricted to a small portion of the spatial domain. The two conditions are illustrated by the shaded region and bold line in the normalized variable diagram shown in Fig. 2.

D. Interpolation Schemes

1. *Step Scheme*

The simplest scheme, the first-order step scheme, involves only the upstream nodal value:

$$I_f = I_C \tag{12}$$

The corresponding NVF for the scheme is

$$\tilde{I}_f = \tilde{I}_C \tag{13}$$

This scheme is unconditionally bounded and is computationally inexpensive, but has the disadvantage of being only first-order accurate.

2. *Diamond Difference Scheme*

The diamond difference (DD) scheme[21] may be represented by the following interpolation:

$$I_f = I_C + I_C - I_{\text{uf}} \tag{14}$$

The subscript uf denotes the face value on the upstream side

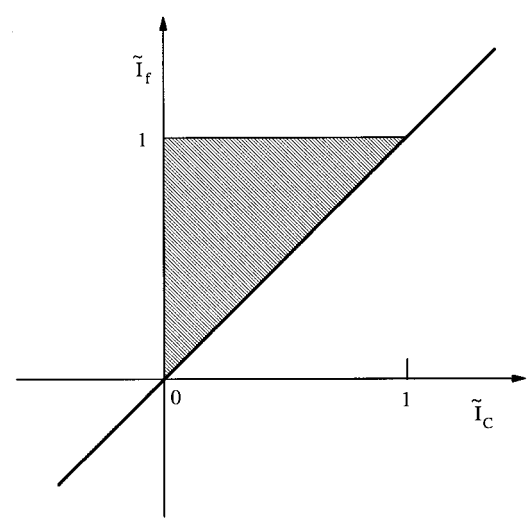

Fig. 2 Normalized variable diagram indicating boundedness criteria.

of node C, as depicted in Fig. 1. The DD scheme differs from the other schemes in this study in that the interpolation at a face is explicitly dependent on fluxes at the upstream face. For this reason, the scheme is left in its unnormalized form. The DD scheme is formally second-order and resembles the central difference scheme. Unfortunately, it is unbounded and may lead to nonphysical over- and undershoots.[5] Several modifications have been proposed in literature to compensate for this undesirable property, but none have been totally satisfactory. Simple solutions include setting face fluxes to zero,[22] and applying a variable weight scheme[23] that shifts the interpolation toward the step scheme. Although both methods eliminate negative intensities, boundedness is not guaranteed, and accuracy is often unnecessarily compromised.

To ensure boundedness, the DD scheme may be reformulated with the universal limiter of Leonard.[13] However, because of the extrapolative nature of the DD scheme, first-order downwind clipping will be necessary to satisfy the boundedness conditions in portions of the domain. This characteristic is shared by the bounded OSHER scheme,[24] which has been found by the authors to converge poorly for RTE applications. For this reason, the proposed bounded DD scheme is not considered in this work.

3. *Bounded HR Schemes*

To simultaneously provide high-order accuracy and maintain boundedness, HR schemes with built-in flux limiters may be used. These schemes are generally based on composite flux expressions. The term composite refers to the piecewise nature of these functions; they are generally constructed from several functions, each valid over an individual range of $\tilde{I}_C$. In the monotonic region ($0 \leq \tilde{I}_C \leq 1$), the face value is obtained from high-order interpolation, whereas outside this region the unconditionally bounded upwind (step) scheme is used. The composite flux expressions are functions of the dependent variable $\tilde{I}_C$, making the schemes nonlinear. A generalization of this family of schemes is presented by Leonard.[13]

Four bounded, HR schemes are considered: 1) Roe's MINMOD (Ref. 25), 2) Van Leer's MUSCL (Ref. 26) and CLAM (Ref. 27), and Gaskell and Lau's SMART (Ref. 20). The normalized variable form of the CLAM scheme is

$$\tilde{I}_f = \begin{cases} \tilde{I}_C(2 - \tilde{I}_C) & \text{for} \quad 0 < \tilde{I}_C < 1 \\ \tilde{I}_C & \text{elsewhere} \end{cases} \tag{15}$$

Expressions for the three other HR schemes are included in the Appendix for completeness. Descriptions may also be found in the original references or in Darwish and Moukalled.[19] The MINMOD, MUSCL, and CLAM schemes are second order, whereas the SMART scheme is third order.

Near boundaries, special treatment is required because of reduced stencils. At faces that are located one control volume from upstream boundaries, the given HR scheme is applied by taking the upstream value I_U to be the boundary value, and by making an associated adjustment in weighting factors for the reduced grid spacing. At faces coincident with downstream boundaries, an upwind scheme is used. The treatment at downstream boundaries may degrade the accuracy of the higher-order operators when strong intensity gradients are encountered at these locations. A bounded, higher-order formulation for downstream boundaries should be developed in the future.

E. Solution Methods

The spatially discrete transport equations are obtained by substituting the corresponding flux expressions [given in general by Eq. (7)] into Eq. (6), and may be denoted by

$$K_m(\boldsymbol{I}_m) = \boldsymbol{F}_m \quad \text{for} \quad m = 1, \ldots, M \tag{16}$$

where K_m is a $N \times N$ matrix representing the discrete form of the continuous transport operator L_m; $\boldsymbol{I}_m$ is the solution vector for the mth ordinate direction; and $\boldsymbol{F}_m$ is a vector that contains volumetric emission and in-scattering terms, and upstream boundary conditions. For the HR schemes, $\boldsymbol{K}_m$ is dependent on $\boldsymbol{I}_m$. Coupling between directions is incorporated in $\boldsymbol{F}_m$ through in-scattering and wall reflection terms.

For the step scheme, Eq. (16) may be solved very efficiently by using a single sweep over the grid in which volumes are visited from upstream to downstream. The process is analogous to ordering the equations for upstream to downstream to provide an upper triangular matrix, and then backsolving the system of equations. This is a characteristic of any interpolation operator that represents face fluxes solely in terms of upstream nodal values. The standard diamond difference scheme possesses this property, even though it has intermediate face flux calculations interwoven in the calculation of the nodal values, i.e., extrapolation to the faces. In the overall solution process, Eq. (16) is individually solved for each ordinate direction, the in-scattering and reflection terms are updated, and the equations are solved again. Iteration continues until convergence is obtained. When high scattering coefficients and/or high wall reflectivities are encountered, solutions may be accelerated via rebalance techniques.[28]

The HR schemes are nonlinear and must be handled differently. A defect correction procedure[29] is applied in which a low-order operator is treated implicitly, while the difference between the HR and the low-order operator is treated explicitly

$$K_m^1(\boldsymbol{I}_m)^{n+1} = [K_m^1(\boldsymbol{I}_m) - K_m^{\mathrm{HR}}(\boldsymbol{I}_m)]^n + \boldsymbol{F}_m \quad \text{for} \quad m = 1, \ldots, M \tag{17}$$

where K_m^1 and K_m^{HR} represent transport operators for the low-order and HR schemes, respectively, and n is the global iterate over the space–angle grid. This approach reduces the computational stencil, but also necessitates iteration to obtain the high-order solution to the ordinate equation. In this work, the low-order operator is taken as the step scheme, and the corresponding sweeping procedure is retained. Consequently, the solution of the discretized ordinate equation is the same for all operators, except for the presence of an explicit defect correction term in the HR schemes. For the HR operators, one flux calculation is made per global iteration or space–angle sweep. Thus, global iterations for all of the schemes are computationally similar and require comparable CPU time.

IV. Results

The differencing schemes are investigated by considering three cases: 1) a black enclosure with a step change in wall emissive power, 2) a rectangular enclosure with a purely absorbing medium, and 3) a rectangular enclosure with a purely scattering medium.

The first case was chosen to graphically illustrate the nature of the differencing schemes. The other two cases are standard benchmark cases. For these cases, the evaluation of the schemes is based on the following criteria: 1) accuracy, 2) boundedness, and 3) convergence characteristics.

The results are compared to available exact and grid-independent solutions. Convergence is measured by the normalized difference in the incident energy from two successive space–angle sweeps:

$$\|R\|_\infty \equiv \max(R_i: \quad i = 1, \ldots, N_{\mathrm{cell}}) < 10^{-6} \tag{18a}$$

where

$$R_i = \frac{\left|G_i^{n+1} - G_i^n\right|}{G_i^{n+1}} \tag{18b}$$

and the superscripts n and i denote the iterate and cell index, respectively. The level-symmetric even S_6 ordinate set[17] was used for all cases, unless otherwise indicated.

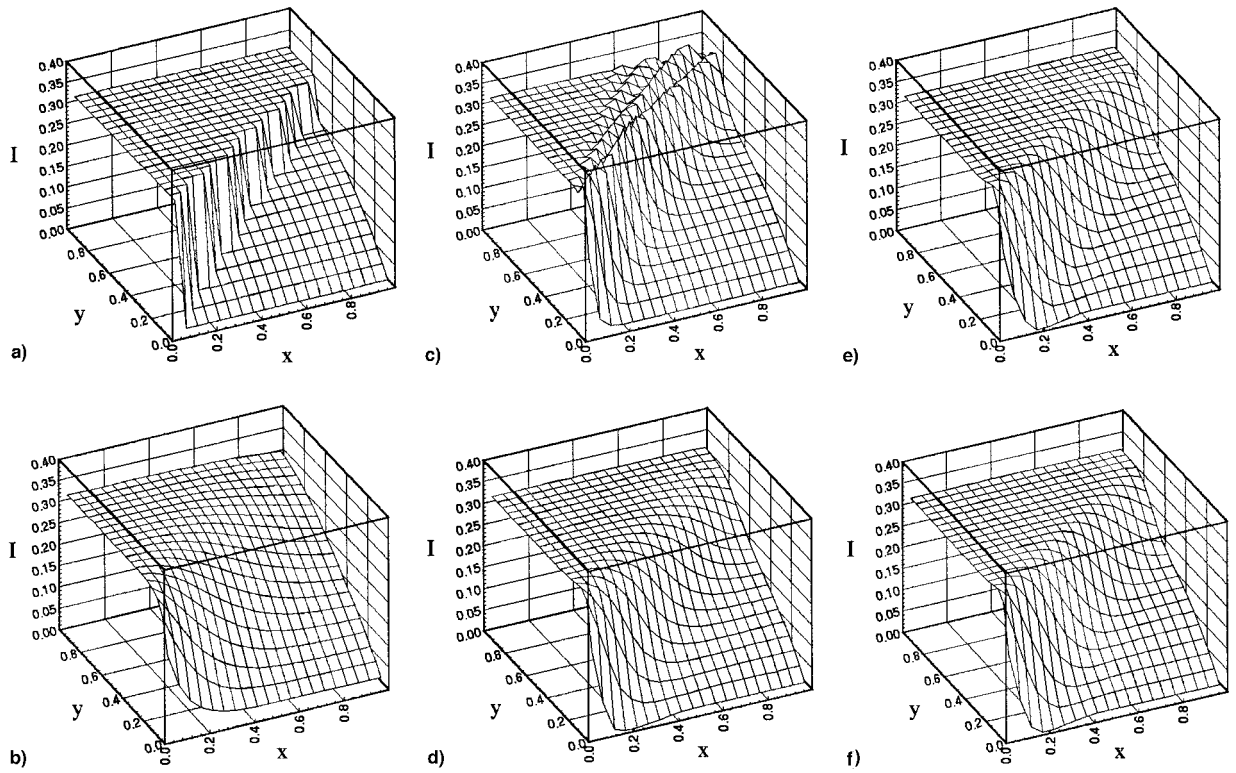

Fig. 3 Intensity in direction $\mu = 0.8040087$, $\xi = 0.5773503$ for case 1: a) exact, b) step, c) diamond difference, d) MINMOD, e) MUSCL, and f) CLAM.

A. Rectangular Enclosure with a Step Change in Wall Emissive Power

A rectangular enclosure with black walls and a purely absorbing medium ($\kappa = 1$) is maintained at an emissive power of unity. All walls are cold except for the one at $x = 0$, which has an emissive power of 1. The case was analyzed with the S_8 quadrature set from Fiveland.[5]

The relative merits of the differencing schemes are illustrated by considering the transport equation for an ordinate direction leaving the hot surface. Figure 3 displays the intensity in direction $\mu = 0.8040087$, $\xi = 0.5773503$, for the various schemes along with the spatially exact solution in the given direction. All results are for a 20 × 20 grid. Because the media is at the same temperature as the hot wall, rays leaving the hot surface maintain a constant intensity. In contrast, rays leaving the cold surface increase in intensity along the ordinate direction path because of emission by the media. A discontinuity, which is caused by the discontinuity in wall emissive power, originates at point (0,0), and continues along the line of the ordinate direction, decreasing with distance. As seen in Fig. 3b, the step scheme smears the solution greatly. The DD scheme, on the other hand, captures the gradient closely, but produces a number of overshoots. In contrast, all bounded schemes capture the steep gradient to a large degree and prevent oscillations.

B. Rectangular Enclosure with an Absorbing Medium

The case consists of a two-dimensional, rectangular enclosure with cold walls and a purely absorbing medium maintained at an emissive power of unity.[2,10] An absorption coefficient κ of 1 is considered.

For black walls, spatially exact solutions to the S_n equations are available.[30] This is not the exact solution to the RTE, but the spatially exact solution to the angular approximation. Therefore, it may be used to measure the error due solely to a given spatial approximation. SD error is quantified with the following error definition:

$$E(x, y) = \frac{|G(x, y) - \bar{G}(x, y)|}{\bar{G}(x, y)} \times 100\% \tag{19}$$

where $\bar{G}$ and G represent the spatially exact and approximate DO solutions, respectively. A single measure is provided by the following norm:

$$\|E\|_1 = \sum V_i E_i \Big/ \sum V_i \tag{20}$$

The summations in Eq. (20) extend over all cells in the computational domain.

The case was analyzed with the various differencing schemes on uniform grids of 10 × 10, 20 × 20, 40 × 40, 80 × 80, and 160 × 160. Accuracy results are shown in Table 1, which displays the L_1 error norm and the predicted spatial approximation order. The predicted order is shown in parentheses and is given by

$$p_{k-1,k} = \frac{\log(e_{k-1}/e_k)}{\log(\Delta x_{k-1}/\Delta x_k)} \tag{21}$$

where the value e denotes any suitable error norm, and the subscripts $k - 1$ and k refer to two grids of differing refinement. Equation (21) was derived by assuming the error is related by the expression $e_k = C\Delta x_k^p$, where C is a constant that is independent of grid size, and p is the order of the method. The error norm results are also graphically displayed in Fig. 4. Because the axes in this plot are both logarithmically scaled, the slope of each curve indicates the predicted order for the given scheme.

As shown in Fig. 4, the error from the step scheme is very high, as expected, and decreases with decreasing grid size in a rate slightly less than the theoretical first-order value (see values in parentheses in Table 1). The error from the DD scheme is much improved over the step scheme, whereas the results from the HR schemes are even better. Although the DD is formally second-order, the method is not as accurate as the bounded second-order schemes. This outcome probably results from oscillations in the DD solutions. The MINMOD, CLAM, and MUSCL schemes have predicted orders slightly less than

Table 1 $\|E\|_1$ error norm for case 2 ($\kappa = 1$)

Grid	Step	DD	MINMOD	MUSCL	CLAM	SMART
10 × 10	3.140	1.309	0.7102	0.7186	0.7102	0.706
20 × 20	2.041	0.3878	0.2411	0.2254	0.2411	0.2684
	(0.6)	(1.8)	(1.6)	(1.7)	(1.6)	(1.4)
40 × 40	1.201	0.1354	0.0778	0.0617	0.0778	0.0948
	(0.8)	(1.5)	(1.6)	(1.9)	(1.6)	(1.5)
80 × 80	0.6775	0.0572	0.0292	0.0241	0.0290	0.0394
	(0.8)	(1.2)	(1.4)	(1.4)	(1.4)	(1.3)
160 × 160	0.3718	0.0260	0.00107	0.0083	0.0107	0.0170
	(0.9)	(1.1)	(1.4)	(1.5)	(1.4)	(1.2)

Note: values in parentheses indicate predicted spatial approximation order.

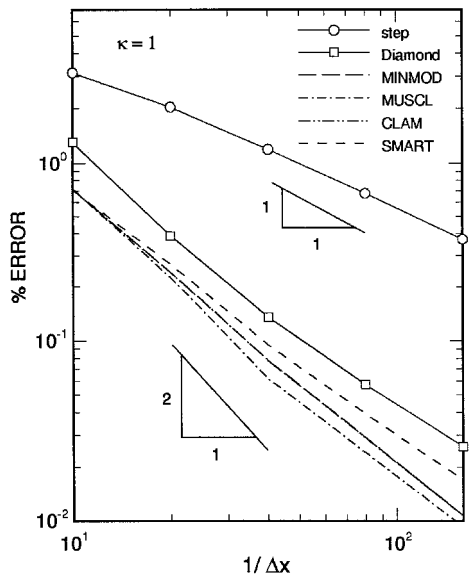

Fig. 4 Reduction in spatial discretization error $\|E\|_1$ resulting from grid refinement for case 2 ($\kappa = 1$). Slope indicates observed order of the differencing scheme.

their theoretical values of 2. Interestingly, the third-order SMART scheme performs similarly to the second-order schemes, and falls well short of the third-order expectations. This discrepancy is probably caused by 1) the limiting required to prevent oscillations, and/or 2) the unalignment of the stencils with respect to the ordinate directions. The effects of the second cause may be reduced by resorting to a skewed upwind-type formulation.[31] Also, the order of a given scheme denotes local truncation error. Because of the one-way nature of the ordinate equation, local error accumulates as the direction is traversed downstream. If upstream fluxes are limited, the lower-order approximation will influence the global accuracy at all downstream locations, and may degrade the observed accuracy of the scheme.

Convergence characteristics are illustrated in Fig. 5 for a 20 × 20 grid and a wall emissivity of 0.5. As expected, the step scheme converges the best; the convergence is controlled solely by the explicitly treated wall reflection terms. The DD results are not shown, but are similar to the step scheme convergence. The convergence rates for the HR schemes are lower than either the step or DD schemes. The difference is attributed to the nonlinearity of the schemes. Convergence rates for all HR schemes are similar to a point, and then the rates for the MINMOD and SMART schemes deteriorate. This degradation is probably caused by the composite interpolation functions. Because the schemes are nonlinear, the interpolation varies with global iteration. Solutions from successive iterations are likely bouncing back and forth between two regions of the composite function, or between limited and nonlimited regions, causing the poor convergence. The CLAM scheme, which has only a single function in monotonic range, performs

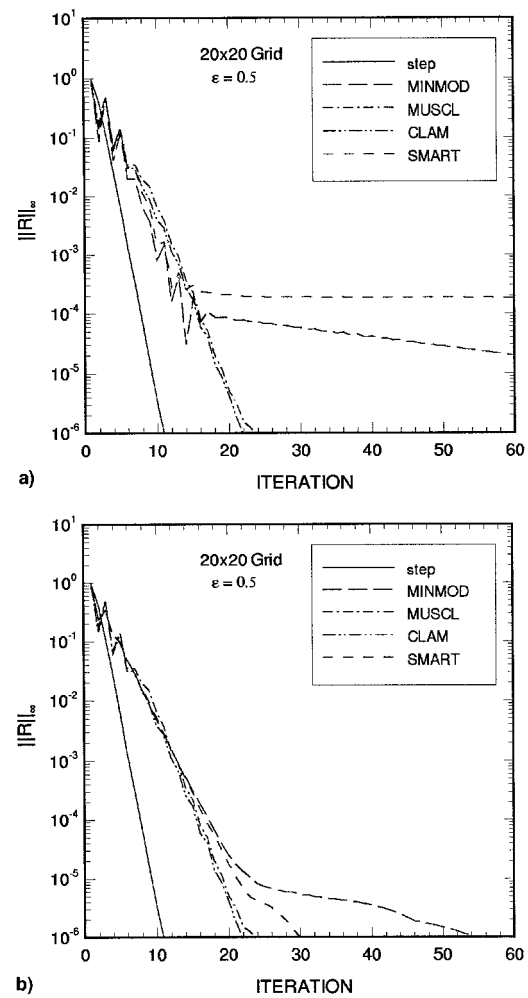

Fig. 5 Convergence histories for case 2 ($\varepsilon = 0.5$, 20 × 20 grid): a) original convergence with no relaxation and b) revised convergence with relaxation.

much better than the MINMOD and SMART schemes. Underrelaxation, applied by damping the residuals in a correction form of Eq. (17), has been found to stabilize the solution of the HR operators, and permit convergence to the 10^{-6} threshold. A damping or relaxation factor of 0.7 was used for the cases that did not converge originally. Revised results with underrelaxation on the MINMOD and SMART schemes are shown in Fig. 5b.

Table 2 displays the total CPU time for the step and CLAM schemes. Results are given for the same conditions as Fig. 5. Slight underrelaxation was required for the 160 × 160 grid. Several conclusions may be drawn from the table. First, the HR scheme, CLAM, requires some overhead for evaluating the limited flux values and for forming the defect correction term [see Eq. (17)]. As shown by the values in parentheses,

the overhead per iteration is approximately 22%, and is generally independent of grid size. Secondly, the nonlinearity of the HR scheme slows convergence. For coarse grids, the CLAM scheme requires about twice as many global iterations as the step scheme. This ratio increases slightly as the grid is refined. Future work on accelerating the convergence of nonlinear schemes will greatly advance their acceptance and use.

C. Rectangular Enclosure with a Purely Scattering Medium

The case consists of a square enclosure with black walls and an isotopically scattering medium.[2,28,32] The lower wall has an emissive power of unity, and the other walls have zero emissive power. All walls of the enclosure have an emissivity of 1. Since exact solutions are not available to this problem, the spatial discretization error is measured by comparing DO results to those from a 320 × 320 uniform grid and the CLAM scheme. This solution is taken as the benchmark to which all other solutions are compared using the error norm of Eq. (20).

The case was analyzed on a number of uniform grids with the various differencing schemes. For a scattering coefficient of 5, error results are shown in Table 3 and Fig. 6. These results are similar to those of the previous absorption case. The exception is that the DD scheme produces lower error norms than the HR schemes at coarse discretizations. Nevertheless, the HR schemes consistently have higher predicted spatial approximation orders and provide higher accuracy on finer grids. The predicted spatial orders mirror the absorption case results. Theoretical orders are not obtained by any scheme.

Convergence characteristics for the schemes are shown in Fig. 7. All results are shown for a 20 × 20 grid and a scattering coefficient of 5. The SMART and MUSCL schemes require slight underrelaxation to achieve convergence. Again, the step scheme converges the best, but the HR schemes perform almost as well because of the apparent domination of the in-scattering terms. Additional analyses have shown that the influence of the HR schemes on convergence and the degree of needed underrelaxation depend somewhat on the optical thickness of the media. The CLAM scheme has proven the most robust. This is likely a result of the C^1 continuity of the interpolation function with respect to the nodal values in the monotonic range, i.e., the interpolation function and its first derivative are continuous.

Table 2 Timing statistics for case 2 ($\kappa = 1$, $\varepsilon = 0.5$)

	Step		CLAM	
Grid	Iterations	CPU time[a]	Iterations	CPU time[a]
10 × 10	11	0.93	25	2.5 (22)
20 × 20	11	3.00	22	7.38 (21)
40 × 40	11	11.5	25	32.3 (23)
80 × 80	12	51.8	31	164.2 (22)
160 × 160	12	210.9	44	951.5 (23)

[a]CPU time is in arbitrary time units.
Note: Values in parentheses are percent overhead/iteration for HR schemes.

Table 4 shows a comparison of CPU time for the step and CLAM schemes for a range of optical thicknesses. The CLAM scheme requires between 35–80% more CPU time as the step scheme over the range. At high optical thicknesses, both schemes require an excessive number of iterations because of the dominance of the in-scattering terms. All schemes should benefit from the use of rebalance acceleration techniques.[28]

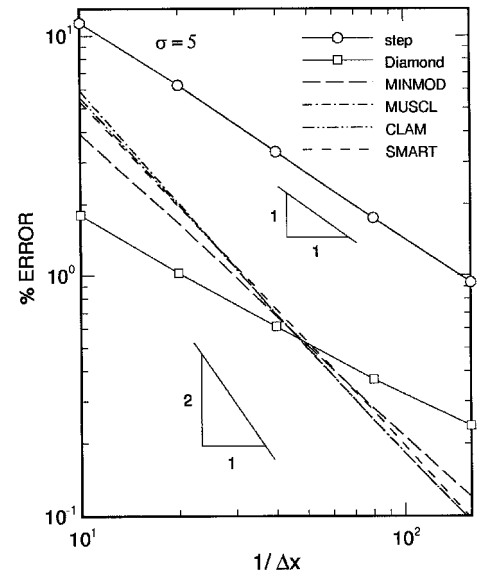

Fig. 6 Reduction in spatial discretization error $\|E\|_1$, resulting from grid refinement for case 3 ($\sigma = 5$). Slope indicates observed order of the differencing scheme.

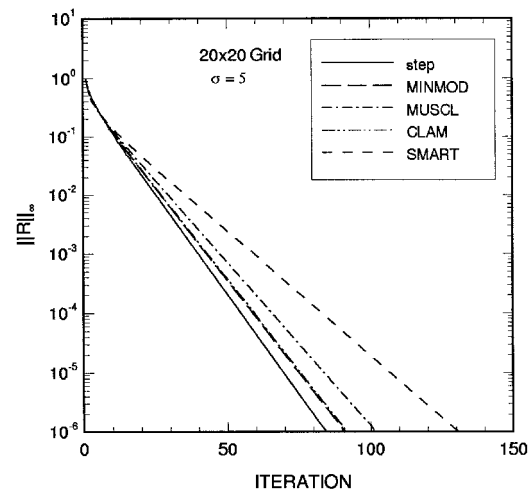

Fig. 7 Convergence histories for case 3 ($\sigma = 5$, 20 × 20 grid).

Table 3 $\|E\|_1$ error norm for case 3 ($\sigma = 5$)

Grid	Step	DD	MINMOD	MUSCL	CLAM	SMART
10 × 10	11.35	1.830	3.913	5.905	5.541	5.332
20 × 20	6.243	1.026	1.673	2.035	2.000	1.973
	(0.9)	(0.8)	(1.2)	(1.5)	(1.5)	(1.4)
40 × 40	3.313	0.6121	0.6774	0.6844	0.6895	0.7218
	(0.9)	(0.7)	(1.3)	(1.6)	(1.5)	(1.5)
80 × 80	1.756	0.3690	0.2803	0.2502	0.2496	0.2722
	(0.9)	(0.7)	(1.3)	(1.5)	(1.5)	(1.4)
160 × 160	0.9376	0.2377	0.1200	0.0879	0.0879	0.0936
	(0.9)	(0.6)	(1.2)	(1.5)	(1.5)	(1.5)
320 × 320	——	——	——	——	0.0[a]	——

[a]Benchmark solution.
Note: Value in parentheses indicates predicted spatial approximation order.

Table 4 Timing statistics for case 3 (20 × 20 grid)

	Step		CLAM	
σ	Iterations	CPU time[a]	Iterations	CPU time[a]
1	19	5.18	28	9.30
5	85	23.4	92	31.1
10	203	55.2	246	81.9

[a]CPU time is in arbitrary time units.

V. Summary

A new approach for spatial discretization of the RTE has been formulated and presented. The present work is intended to serve as a bridge between historical and contemporary methods and to provide a foundation for future schemes. By maintaining low numerical smearing and dispersion, the investigated HR schemes show dramatic improvement in accuracy over the step scheme while providing boundedness lacked by conventional second-order schemes. The nonlinearity of the HR schemes often necessitates an increase in global iterations. Nevertheless, for significantly scattering media or reflective walls, the HR schemes are competitive with the standard differencing schemes with respect to CPU time.

In addition to the presented HR schemes, other bounded schemes may be investigated using the NVF and monotonicity-maintenance criteria. Such schemes include, but are not limited to, bounded forms of the exponential[22] and skewed upwind[31] schemes. Initial extensions to the skewed upwind scheme for radiative heat transfer have already been made by Raithby and Chui[8] and Chai et al.[9] As for unidirectional implementations, ones in which the interpolation stencil is aligned with the grid, little utility will likely be gained from increasing the order above second, as illustrated by the SMART scheme results. One of the most promising methods will probably be a bounded exponential or high-order scheme in which the interpolation stencil is aligned with the ordinate direction.

With the spatial discretization methods presented in this paper, angular differencing practices may now be objectively investigated. The accuracy of S_n quadratures and various other approximations may be accessed without fear of contamination of results from the spatial approximation. Future work should focus on improving angular differencing practices to reduce ray effects. Possible candidates are high-order, angular, finite element or finite angle approximations. These approximations will likely require techniques similar to those presented here to provide boundedness. Lastly, the spatial HR schemes should be applied to three-dimensional geometries and to anisotropically scattering and nongray media.

Appendix: Composite HR Functions

The functions representing the MINMOD, MUSCL, and SMART schemes are shown next.

MINMOD:

$$\tilde{I}_f = \begin{cases} \frac{3}{2}\tilde{I}_C & \text{for} \quad 0 < \tilde{I}_C \leq \frac{1}{2} \\ \frac{1}{2}(1 + \tilde{I}_C) & \text{for} \quad \frac{1}{2} < \tilde{I}_C < 1 \\ \tilde{I}_C & \text{elsewhere} \end{cases} \tag{A1}$$

MUSCL:

$$\tilde{I}_f = \begin{cases} 2\tilde{I}_C & \text{for} \quad 0 < \tilde{I}_C \leq \frac{1}{4} \\ \frac{1}{4} + \tilde{I}_C & \text{for} \quad \frac{1}{4} < \tilde{I}_C \leq \frac{3}{4} \\ 1 & \text{for} \quad \frac{3}{4} < \tilde{I}_C < 1 \\ \tilde{I}_C & \text{elsewhere} \end{cases} \tag{A2}$$

SMART:

$$\tilde{I}_f = \begin{cases} 3\tilde{I}_C & \text{for} \quad 0 < \tilde{I}_C \leq \frac{1}{6} \\ \frac{3}{8} + \frac{3}{4}\tilde{I}_C & \text{for} \quad \frac{1}{6} < \tilde{I}_C \leq \frac{5}{6} \\ 1 & \text{for} \quad \frac{5}{6} < \tilde{I}_C < 1 \\ \tilde{I}_C & \text{elsewhere} \end{cases} \tag{A3}$$

References

[1]Lewis, E. E., and Miller, W. F., *Computational Methods of Neutron Transport*, Wiley, New York, 1984.

[2]Fiveland, W. A., "Discrete-Ordinates Solutions of the Radiative Transport Equation for Rectangular Enclosures," *Journal of Heat Transfer*, Vol. 106, No. 4, 1984, pp. 699–706.

[3]Briggs, L. L., Miller, W. F., and Lewis, E. E., "Ray-Effect Mitigation in Discrete Ordinate-Like Angular Finite Element Approximations in Neutron Transport," *Nuclear Science and Engineering*, Vol. 57, No. 3, 1975, pp. 205–217.

[4]Paternoster, R. R., and Walters, W. F., "The Nodal Transport Method for General Triangular Meshes in (X,Y)-Geometries," *Progress in Nuclear Energy*, Vol. 18, Nos. 1/2, 1986, pp. 153–160.

[5]Fiveland, W. A., "Three-Dimensional Radiative Heat Transfer Solutions by the Discrete-Ordinates Method," *Journal of Thermophysics and Heat Transfer*, Vol. 2, No. 4, 1988, pp. 309–316.

[6]Truelove, J. S., "Discrete-Ordinates Solutions of the Radiation Transport Equation," *Journal of Heat Transfer*, Vol. 109, No. 4, 1988, pp. 1048–1051.

[7]Fiveland, W. A., and Jessee, J. P., "A Finite Element Formulation of the Discrete Ordinates Method for Multidimensional Geometries," *Journal of Thermophysics and Heat Transfer*, Vol. 8, No. 3, 1994, pp. 426–433.

[8]Raithby, G. D., and Chui, E. H., "A Finite-Volume Method for Predicting a Radiant Heat Transfer in Enclosures with Participating Media," *Journal of Heat Transfer*, Vol. 112, No. 2, 1990, pp. 415–423.

[9]Chai, J. C., Lee, H. S., and Patankar, S. V., "Finite Volume Method for Radiation Heat Transfer," *Journal of Thermophysics and Heat Transfer*, Vol. 8, No. 3, 1994, pp. 419–425.

[10]Fiveland, W. A., and Jessee, J. P., "A Comparison of Discrete Ordinates Formulations for Radiative Heat Transfer in Multidimensional Geometries," *Journal of Thermophysics and Heat Transfer*, Vol. 9, No. 1, 1995, pp. 47–54.

[11]Lathrop, K. D., "Ray Effects in the Discrete Ordinates Equations," *Nuclear Science and Engineering*, Vol. 32, 1968, pp. 357–369.

[12]Chai, J. C., Lee, H. S., and Patankar, S. V., "Ray Effect and False Scattering in the Discrete Ordinates Method," *Numerical Heat Transfer, Part B*, Vol. 24, No. 4, 1993, pp. 373–389.

[13]Leonard, B. P., "The ULTIMATE Conservation Difference Scheme Applied to Unsteady One-Dimensional Advection," *Computer Methods in Applied Mechanics and Engineering*, Vol. 88, No. 1, 1991, pp. 17–74.

[14]Darwish, M. S., "A New High Resolution Scheme Based on the Normalized Variable Formulation," *Numerical Heat Transfer, Part B*, Vol. 24, 1993, pp. 287–307.

[15]Alcouffe, R. E., "An Adaptive Weighted-Diamond Differencing Method for XYZ Geometry," *Transactions of the American Nuclear Society*, Vol. 68A, 1993, pp. 206–209.

[16]Germogenova, T. A., Shwetsov, A. V., and Voloschenko, A. M., "Adaptive Positive Nodal Method for Transport Equation," *Transport Theory and Statistical Physics*, Vol. 23, No. 7, 1994, pp. 923–970.

[17]Fiveland, W. A., "The Selection of Discrete Ordinate Quadrature Sets for Anisotropic Scattering," American Society of Mechanical Engineers, HTD-Vol. 72, 1991, pp. 89–96.

[18]Leonard, B. P., "A Survey of Finite Differences with Upwinding for Numerical Modelling of the Incompressible Convection Diffusion Equations," *Computational Techniques in Transient and Turbulent Flow*, edited by C. Taylor and K. Morgan, Vol. 2, Pineridge, Swansea, Wales, UK, 1981, pp. 1–35.

[19]Darwish, M. S., and Moukalled, F. H., "Normalized Variable and Space Formulation Methodology for High Resolution Schemes," *Numerical Heat Transfer, Part B*, Vol. 26, 1994, pp. 79–96.

[20]Gaskell, P. H., and Lau, A. K. C., "Curvature Compensated Convective Transport: SMART, a New Boundedness Preserving Transport Algorithm," *International Journal for Numerical Methods in Fluids*, Vol. 8, No. 6, 1988, pp. 617–641.

[21]Lathrop, K. D., "Use of Discrete-Ordinate Methods for Solution of Photon Transport Problems," *Nuclear Science and Engineering*, Vol. 24, 1966, pp. 381–388.

[22]Carlson, B. G., and Lathrop, K. D., *Transport Theory—The Method of Discrete-Ordinates in Computing Methods in Reactor Physics*, edited by H. Greenspan, C. Kelber, and D. Okrent, Gordon and Breach, New York, 1968.

[23]Jamaluddin, A. S., and Smith, P. J., "Predicting Radiative Transfer in Axisymmetric Cylindrical Enclosures Using the Discrete Ordinates Method," *Combustion Science and Technology*, Vol. 62, Nos. 4–6, 1988, pp. 173–186.

[24]Chakravarthy, S. R., and Osher, S., "High Resolution Application

of the OSHER Upwind Scheme for the Euler Equations," AIAA Paper 83-1943, 1983.

[25]Harten, A., "High Resolution Schemes for Hyperbolic Conservation Laws," *Journal of Computational Physics*, Vol. 49, No. 3, 1983, pp. 357–393.

[26]Van Leer, B., "Towards the Ultimate Conservation Difference Scheme. V. A Second-Order Sequel to Godunov's Method," *Journal of Computational Physics*, Vol. 32, 1977, pp. 101–136.

[27]Van Leer, B., "Towards the Ultimate Conservation Difference Scheme. II. Monotonicity and Conservation Combined in a Second-Order Scheme," *Journal of Computational Physics*, Vol. 14, 1974, pp. 361–370.

[28]Fiveland, W. A., and Jessee, J. P., "Acceleration Schemes for the Discrete Ordinates Method," *Journal of Thermophysics and Heat Transfer*, Vol. 10, No. 3, 1996, pp. 445–451.

[29]Böhmer, K., Hemker, P. W., and Stetter, H. J., "The Defect Correction Approach," *Computing, Supplement 5, Defect Correction Methods*, edited by K. Böhmer and H. J. Stetter, 1984, pp. 1–32.

[30]Jessee, J. P., Howell, L. H., Fiveland, W. A., Colella, P., and Pember, R. B., "An Adaptive Mesh Refinement Algorithm for the Discrete Ordinates Method," *Proceedings of the 31st National Heat Transfer Conference*, HTD-Vol. 325, 1996, pp. 115–124.

[31]Raithby, G. D., "Skew Upstream Differencing Schemes for Problems Involving Fluid Flow," *Computer Methods in Applied Mechanics and Engineering*, Vol. 9, No. 2, 1976, pp. 153–164.

[32]Ratzel, A. C., and Howell, J., "Two Dimensional Radiation in Absorbing-Emitting-Scattering Media Using the P-N Approximation," *Journal of Heat Transfer*, Vol. 105, No. 2, 1983, pp. 333–340.